Journal of Volcanology and Geothermal Research 347 (2017) 149–164

Contents lists available at ScienceDirect

Journal of Volcanology and Geothermal Research

journal homepage: www.elsevier.com/locate/jvolgeores

Invited research article

Magma transport and storage at Mt. Etna (Italy): A review of geodetic and petrological data for the 2002–03, 2004 and 2006 eruptions

Mimmo Palano [a,*], Marco Viccaro [a,b], Francesco Zuccarello [b], Stefano Gresta [b]

[a] Istituto Nazionale di Geofisica e Vulcanologia, sezione di Catania - Osservatorio Etneo, Piazza Roma 2, I-95129 Catania, Italy
[b] Università degli Studi di Catania, Dipartimento di Scienze Biologiche, Geologiche e Ambientali, Sezione di Scienze della Terra, Corso Italia 57, I-95129 Catania, Italy

ARTICLE INFO

Article history:
Received 11 May 2017
Received in revised form 7 September 2017
Accepted 17 September 2017
Available online 21 September 2017

Keywords:
Eruptive cycle
Ground deformation
Trace elements
Isotope systematic
Magma storage
Magma transfer
Mt. Etna

ABSTRACT

A detailed reconstruction of magma movements within the plumbing system of Mt. Etna volcano has been made by reviewing the eruptions occurring during the October 2002–December 2006 period. The availability of continuous GPS data allowed detecting at least ten different ground deformation stages, highlighting deflationary and inflationary episodes as well as the occurrence of a shallow dike intrusion. These data have been coupled with the available petrological datasets including major/trace elements and Sr-Nd-Pb isotope compositions for the volcanic rocks erupted in the 2002–2006 period. We identified two main magmatic reservoirs located at different depths along the plumbing system of the volcano. The former is located at a depth of ~7 km bsl and fed the 2001 and 2002–03 eruptions, while the latter, located from 3.5 to 5.5 km bsl, fed the 2004–05 and 2006 eruptions. Petrological characteristics of emitted products have been correlated with the inflation vs. deflation cycles related to the identified sources, providing evidence for changes through time of the evolutionary degree of the erupted magmas along with variations in their geochemical feature. Finally, we suggest that a modification of the deep plumbing system of the volcano might have occurred during the 2002–03 eruption, as a consequence of the major seaward motion of the eastern flank of the volcano.

1. Introduction

Over the last decade, the number of studies integrating multidisciplinary datasets, including geodetic, geochemical, seismological and petrological measurements/observations, has increased. These studies are now becoming a more complete approach to modern volcanology. This improvement has been widely encouraged by the rapid growth of continuously recording geophysical networks, which have enabled acquiring extensive datasets at several active volcanoes worldwide. Valuable examples come from Turrialba (Martini et al., 2010), El Hierro (Martí et al., 2013), Manda Hararo rift (Barnie et al., 2015) and St. Helens (Saunders et al., 2012).

Such kinds of multidisciplinary studies have recently been carried out at Mt. Etna volcano (Fig. 1), providing detailed constraints on subsurface magma storage and conduits, thereby improving our understanding of the dynamics of some recent eruptions (e.g. Kahl et al., 2013; Viccaro et al., 2014, 2016a, 2016b; Cannata et al., 2015; Spampinato et al., 2015). This work aims at providing new constraints on the plumbing system of the volcano and evaluating its evolution over the time. In doing so, we reviewed the August 2001–December 2006 period by taking into account continuous GPS measurements and already published petrological data. The selected period suits such research well since there were three large flank eruptions that ranged in different eruptive styles and regimes, with intensely explosive (2002–03 eruption), moderately explosive (2006 eruption), and exclusively effusive (2004–05 eruption) features.

The main petrological trends of each eruptive event have been extensively studied, and there is a broad consensus among the results reported in literature (Clocchiatti et al., 2004; Andronico et al., 2005; Corsaro et al., 2009; Ferlito et al., 2009, 2012; Giacomoni et al., 2012, 2014; Nicotra and Viccaro, 2012; Kahl et al., 2015). Nonetheless, even considering that a number of papers have already studied the deformation patterns of these eruptive events (e.g. Aloisi et al., 2003; Bruno et al., 2012), not all the different ground deformations affecting the volcano edifice during the selected interval have been analyzed. Moreover, other authors analyzed different time intervals, only based on the availably of episodic GPS measurements and therefore, providing models and interpretations on not entirely homogeneous deformative events (e.g. Bonforte et al., 2007a, 2008). In addition, the different approaches used to compute and model the geodetic dataset do not allow a direct comparison among the obtained results. In order to overcome these problems, we analyzed and modeled the GPS data collected over the selected

* Corresponding author at: Istituto Nazionale di Geofisica e Vulcanologia, Sezione di Catania - Osservatorio Etneo, Piazza Roma, 2, 95129 Catania, Italy.
E-mail address: mimmo.palano@ingv.it (M. Palano).

https://doi.org/10.1016/j.jvolgeores.2017.09.009
0377-0273/

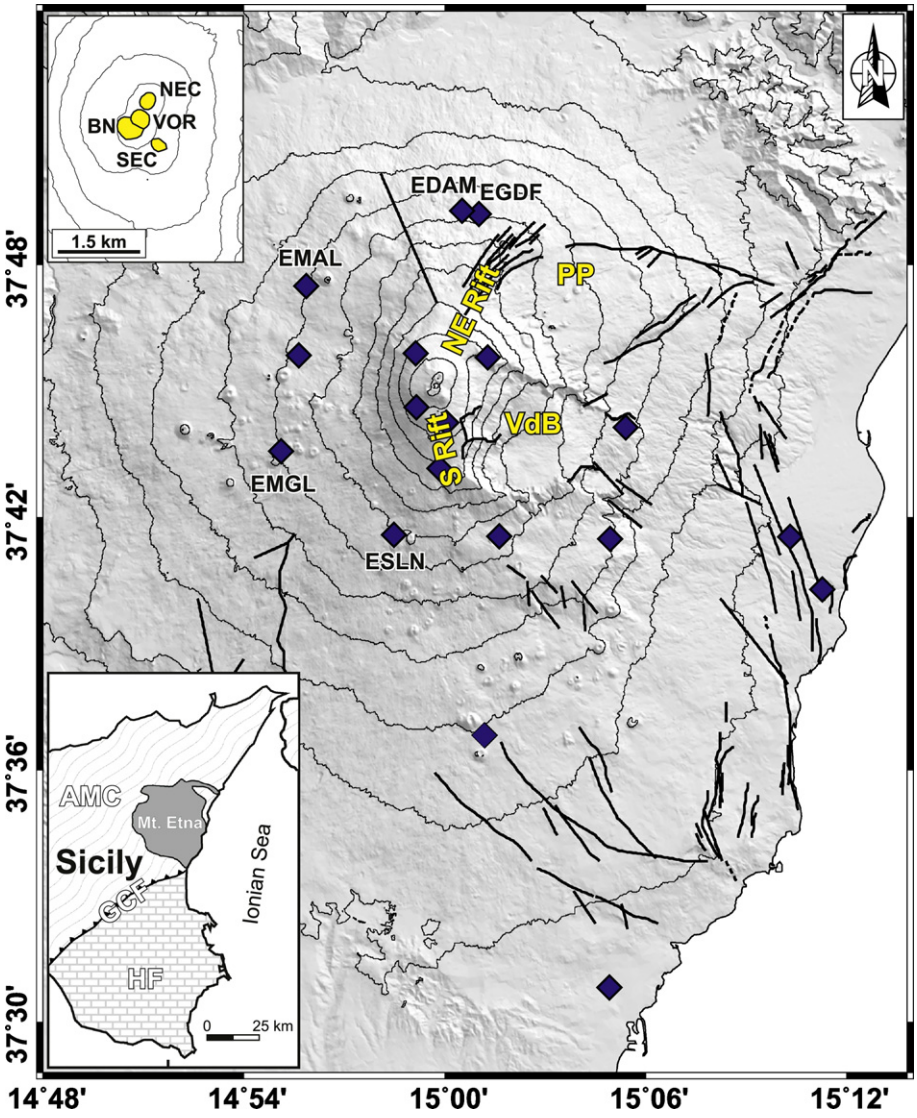

Fig. 1. Simplified tectonic map of Mt. Etna with the location of the GPS stations used in this study; VdB, Valle del Bove; PP, Piano Provenzana. Lower left inset shows a simplified structural map of eastern Sicily and the geographic location of Mount Etna; abbreviations are: AMC, Apennine-Maghrebian chain; GCF, Gela-Catania Foredeep; HF, Hyblean Foreland. Upper left inset show a magnification of the volcano summit craters (Bocca Nuova, BN; Voragine, VOR; North-East Crater, NEC; South-East Crater, SEC).

period by using the same approaches adopted in recent literature at Mt. Etna (e.g. González and Palano, 2014; Cannata et al., 2015, Spampinato et al., 2015; Gambino et al., 2016; Viccaro et al., 2016b).

We anticipate that, by careful inspecting the daily baseline changes of two pairs of GPS stations (Fig. 2), we proposed an unprecedented and detailed resolution of different deformative episodes occurring at Mt. Etna volcano. The surface deformation for each detected stage was used to constrain isotropic half-space elastic inversion models. Finally, the joint interpretation of constraints coming from continuous geodetic data and published petrological observations allowed us to provide a revised model of the time history of magma ascent and interactions between magma batches that have fed the eruptions. In doing this, we confirm some findings reported in literature, also providing a novel interpretation for the specific period of activity here considered.

This study is organized as follows. First, we summarize the background volcanological information for all the three investigated eruptive events. Second, we present the data used and the methods of analysis. Third, we discuss the results and compare the geodetic and petrological observations. Lastly, we summarize all the constraints, resulting from our integrated approach, on the magma transport and storage at Mt. Etna.

2. Background setting

Mt. Etna is an open-vent Quaternary basaltic volcano, located at the front of the Apennine-Maghrebian thrust belt on the east coast of Sicily (Fig. 1). As noted above, during the interval considered in this study, Mt. Etna volcano underwent three large eruptions.

On the evening of 26 October 2002 a seismic swarm, coupled with intense explosive activity the morning after, heralded the onset of the 2002–03 eruption (Andronico et al., 2005). The eruptive activity initially involved the South-Rift of the volcano (hereinafter S-Rift; Fig. 1), where a NS-trending 1.5 km-long eruptive fissure opened at an elevation between 2800 and 2600 m asl. At the same time, a 340 m-long eruptive fissure, oriented ~N10°W and producing weak Strombolian activity, opened at the northern base of Northeast Crater (NEC, Fig. 2 and S1). After a few hours, a new fissure opened along the Northeast Rift (hereinafter NE-Rift; Fig. 1): this fissure was 3.7 km long and propagated, as three main segments, from 2500 down to 1890 m asl in <24 h, striking roughly from N20°E at the upper portion of fracture field to N45°E at the lower elevations (Andronico et al., 2005; Fig. 2). Lava flows were discharged by lower vents eastward reaching the area of Piano Provenzana (Fig. S1) and, almost contemporaneously, on the S-Rift lava started to flow toward SSW reaching an elevation of 1750 m asl

(Fig. 2). The eruption was also characterized by intense explosive activity coupled with abundant ash emission. On the NE-Rift, the eruption stopped on 4 November 2002, while on the S-Rift it lasted for three months, with explosive activity and the formation of a complex lava field, ending on 28 January 2003 (Andronico et al., 2005). It is noteworthy that, on 22 September 2002, a month before the beginning of the 2002–03 eruption, a M = 3.7 earthquake struck the northeastern sector of Mt. Etna as a consequence of seaward motion of the eastern flank of Mt. Etna. Such an event was considered a "broadly preparatory phase" of the eruption onset (Bonforte et al., 2007a).

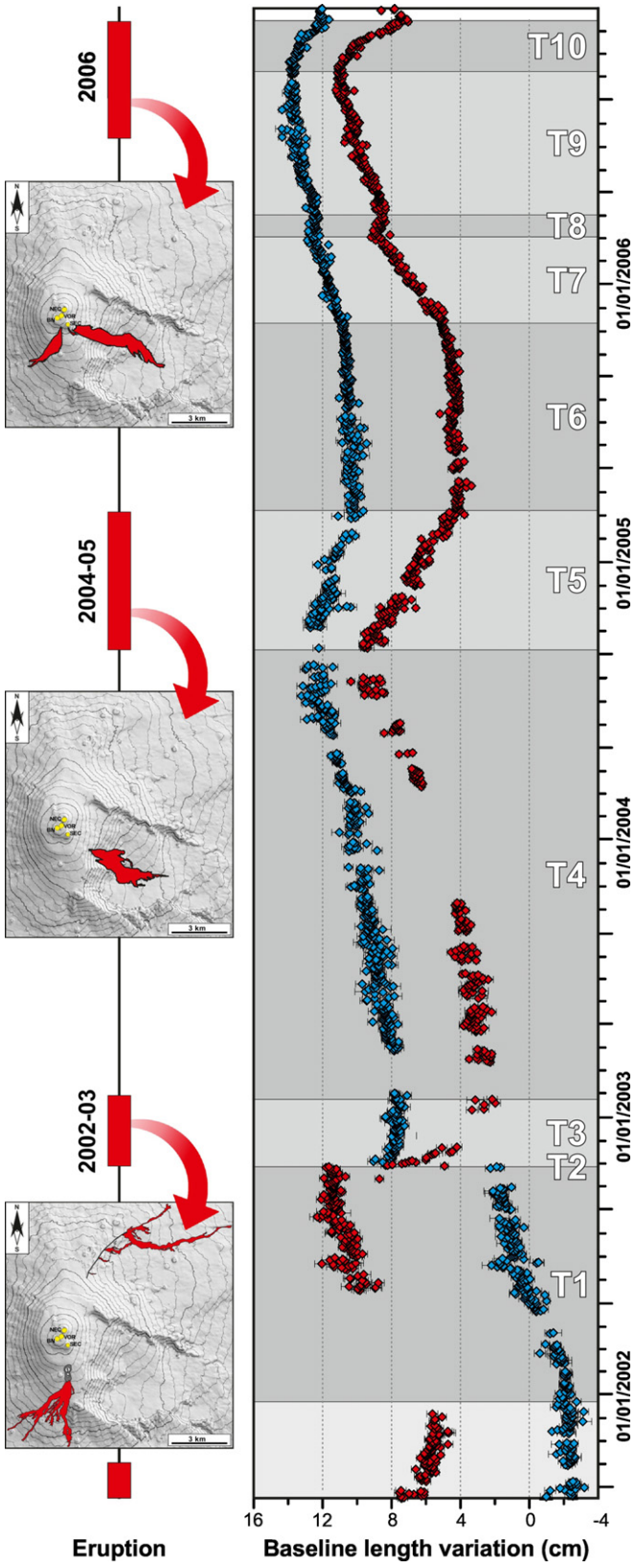

After ~20 months of quiescence, mainly characterized by continuous degassing with occasional explosive activity from the summit craters, on 7 September 2004, volcanic activity resumed with the opening of a 200 m-long radial fissure at the eastern foot of the Southeast Crater (SEC; Fig. 2) at ~3000 m asl (Corsaro and Miraglia, 2005). By midday, a small lava flow emerged from the lowermost portion of this fissure and spread SE toward the Valle del Bove (VdB, Figs. 1 and 2). On 8 September, the lava flow stopped while, from 9 September, a NNW-SSE fracture system opened down to the upper slopes of the VdB (Fig. 1) where lava was emitted from two vents (at altitudes of 2650 and 2350 m, respectively). The eruption continued until early March 2005, leading to the expansion of the lava field downhill to 1670 m elevation within the VdB (Corsaro and Miraglia, 2005).

Volcanic activity restarted at the summit craters during the night of 14 July 2006, when a fissure opened on the eastern flank of the SEC (Fig. 2 and S1). Three vents opened along this fissure: the uppermost vent was characterized by strong degassing and significant Strombolian activity; the lowermost vents (A in Fig. S1) emitted two distinct lava flows which merged together after a few hundred meters and propagated eastward inside the VdB. This eruption ended on 23 July 2006, and several days of sustained degassing activity without ash emission then took place (Kahl et al., 2015). Volcanic activity began again at SEC at the end of August 2006, with Strombolian activity and the formation of new short lava flows expanding eastward for about 1 km; this activity lasted until mid-September. On 13 October 2006, a new eruptive fracture opened from the eastern base of the SEC, reaching an altitude of ~2800 m asl; here, effusive activity started (vent B in Fig. S1) forming lava flows that spread eastward (Kahl et al., 2015). On 23 October, a new eruptive fissure opened on the southern flank of SEC: this fissure (C in Fig. S1) fed some lava flows that propagated toward the south and southeast. On 26 October, a new fracture field formed on the opposite side of the SEC, involving also the southern flank of the Bocca Nuova (BN) crater at 3050 m asl and a new lava flow (D in Fig. S1) was emitted in the SSW direction. Other effusive vents were intermittently active on the SE flanks of SEC (vents E and F in Fig. S1). Only episodic increases in volcanic tremor accompanied the periods characterized by more intense degassing and Strombolian activity at the SEC (Ferlito et al., 2010). The eruption ended on 15 December 2006 (Kahl et al., 2015).

3. GPS data and methods

3.1. Data processing

At Mt. Etna, the GPS permanent network began operating in late 2000 (Fig. 1). Since then, the permanent network has been improved, reaching the current configuration of 39 stations that cover a large part of the volcanic edifice. Available raw GPS observations, covering

Fig. 2. On the left: eruptive events and associated lava fields occurring during the investigated time interval (see also Fig. S1 of the supplementary material section for a magnification of the maps). On the right: daily baseline changes of EDAM-ESLN (red diamonds) and EMGL-EMAL (light-blue diamonds) stations (see the map location in Fig. 1). The time series of EDAM-ESLN baseline is composed as follows: from 15 December 2001 up to 1 July 2003 as EGDF-ESLV baseline, from 1 July 2003 up to 10 October 2004 as EDAM-ESLV baseline and from 11 October 2004 up to 31 December 2006 as EDAM-ESLN baseline, since EDAM and ESLN replaced EGDF and ESLV stations, respectively.

the 15 August 2001–31 December 2006 period, were analyzed using the GAMIT/GLOBK software (Herring et al., 2010) and adopting methodology described in González and Palano (2014). To detect significant changes associated with Mt. Etna activity, as a first step, we inspected the daily baseline changes of two pairs of stations (EDAM-ESLN and EMGL-EMAL) that quasi-continuously operated throughout the investigated period (Fig. 2). The changes over time of these baselines are able to track the magma movement within the volcano plumbing system (e.g. Cannata et al., 2015; Spampinato et al., 2015). The visual inspection of both baselines allows detecting at least ten different ground deformation stages, capturing well deflationary (T3, T5, T8, T10) and inflationary (T1, T4, T6, T7, T9) episodes, as well as the occurrence of a shallow dike intrusion (T2). For each detected stage, in a second step, we estimated the ground deformation field in terms of geodetic velocities by combining the daily GAMIT solutions into a consistent set of station positions and velocities and adopting a local reference frame to isolate the volcanic deformation from the background tectonic pattern (see Palano et al., 2010 for details).

3.2. Data modeling

The surface deformation for each detected stage was used to constrain isotropic half-space elastic inversion models by adopting the same approach described in Cannata et al. (2015). More in detail, the inversions were performed by using the genetic algorithm approach (e.g. Tiampo et al., 2000); in order to include topography, the method of Williams and Wadge (2000) was also adopted. To model the observed ground deformation, the Yang et al.'s (1988) and Okada's (1985) analytical models were used. Values of 30 GPa and 0.25 were assumed for the shear modulus and Poisson's ratio in the half-space, respectively. Estimation of the uncertainties in best fitting parameters was performed by adopting a Jackknife sampling method (Efron, 1982). In the computation, both horizontal and vertical GPS components were inverted by taking into account the weights proportional to the estimated geodetic velocity errors. During the inversions, in order to obtain realistic estimations of the pressure change parameter, we limited the ratio of the pressure change to the shear modulus within the elastic limits of the surrounding rock as suggested by Lisowski et al. (2008). Parameters of best fitting sources are reported in Table 1, while the comparisons between observed and modeled ground deformation are reported in Figs. 3, 4 and 5.

4. Petrological data

A considerable amount of petrological data has been published for the three flank eruptions occurring in the period under investigation. For the purposes of this work, we have selected only the compositional data for the whole rock, basically datasets for major and trace elements, along with Sr-Nd-Pb isotope systematics were available. As concerns the 2002–03 eruption, data have been taken from Clocchiatti et al. (2004) [major/trace elements plus Sr isotope compositions], Ferlito et al. (2009) [major and trace elements] and Ferlito et al. (2012) [major/trace elements plus Sr-Nd-Pb isotope compositions]; data for the 2004–05 eruption are from Corsaro et al. (2009) [major/trace elements plus Sr-Nd isotope compositions] and Ferlito et al. (2012) [data as above]; data for the 2006 eruptive events are from Nicotra and Viccaro (2012) [major/trace elements plus Sr-Pb isotope compositions]. Readers can refer to the cited papers to get specific information on the analytical procedures followed to obtain compositional data for major-trace elements and isotope systematics. Given that all the available data come from different laboratories, readers should be aware that analytical bias is possible. In this regard, data provided by Ferlito et al. (2012) for the 2002–05 period and those of Nicotra and Viccaro (2012) for the 2006 period display the best consistency, given that major/trace elements and isotope data come, respectively, from the same analytical laboratory.

Table 1
Parameters of modeled sources inferred for each interval analyzed in the study. ΔV is expressed as total volume changes. For each parameter, errors (at 95% of confidence) also were reported.

Id	Time interval (dd/mm/yy)	Easting (m)	Northing (m)	Depth (m bsl)	a-axis (m)	a/b ratio	Length (m)	Width (m)	Azimuth (°)	Dip (°)	Pressure (10^8 Pa)	ΔV (10^6 m^3)	Opening (m)
T1	20/12/01–26/10/02	498,735.2 ± 428.8	498,735.2 ± 417.5	6955.0 ± 552.2	1160.1 ± 188.6	0.43 ± 0.08			183.2 ± 5.5	60.1 ± 6.1	8.9 ± 1.5	26.77	
T2	26/10/02–27/10/02	500,880 ± 223.7	4,182,109 ± 320.3	−721.6 ± 341.3			3858.1 ± 318.4	1413.4 ± 412.2	204 ± 7.7	89.9*			2.4 ± 0.7
T3	27/10/02–23/01/03	500,051.6 ± 170.2	4,176,584.4 ± 201.5	4836.5 ± 225.8	1455.3 ± 144.2	0.32 ± 0.07			178.6 ± 7.2	49.7 ± 5.8	−2.1 ± 0.9	−7.3	
T4	23/01/03–07/09/04	498,031.2 ± 228.7	4,178,637.9 ± 359.1	4335.8 ± 448.4	821.4 ± 259.3	0.51 ± 0.12			46.7 ± 4.1	123.2 ± 5.2	8.9 ± 2.1	13.4	
T5	07/09/04–10/03/05	500,147.3 ± 162.9	4,177,396.2 ± 296.3	5450.3 ± 323.7	816.6 ± 284.9	0.62 ± 0.08			58.5 ± 3.4	28.6 ± 4.6	−3.5 ± 1.2	−8.4	
T6	10/03/05–12/11/05	497,404.1 ± 274.4	4,178,426.7 ± 367.6	4804.1 ± 223	631.3 ± 84.6	0.38 ± 0.06			44.8 ± 2.4	120.1 ± 3.1	6.7 ± 1.8	2.5	
T7	12/11/05–06/03/06	499,392.3 ± 275.9	4,178,058.7 ± 261.4	4503.2 ± 476.2	1813.8 ± 293.8	0.52 ± 0.11			81.4 ± 7.3	113.5 ± 4.2	3.7 ± 1.1	6.4	
T8	06/03/06–04/04/06	–	–	–	–	–	–	–	–	–	–	–	–
T9	04/04/06–13/10/06	498,105.8 ± 150.8	4,178,275.3 ± 213.4	5064.9 ± 430.4	1100.2 ± 131.9	0.28 ± 0.12			35.4 ± 4.8	123.0 ± 4.7	4.7 ± 1.9	5.0	
T10	13/10/06–16/12/06	499,609.2 ± 125.4	4,177,852.8 ± 201.9	3662.8 ± 344.5	988.5 ± 228.5	0.4 ± 0.11			140.5 ± 11.2	76.7 ± 6.5	−2.9 ± 0.7	−4.6	

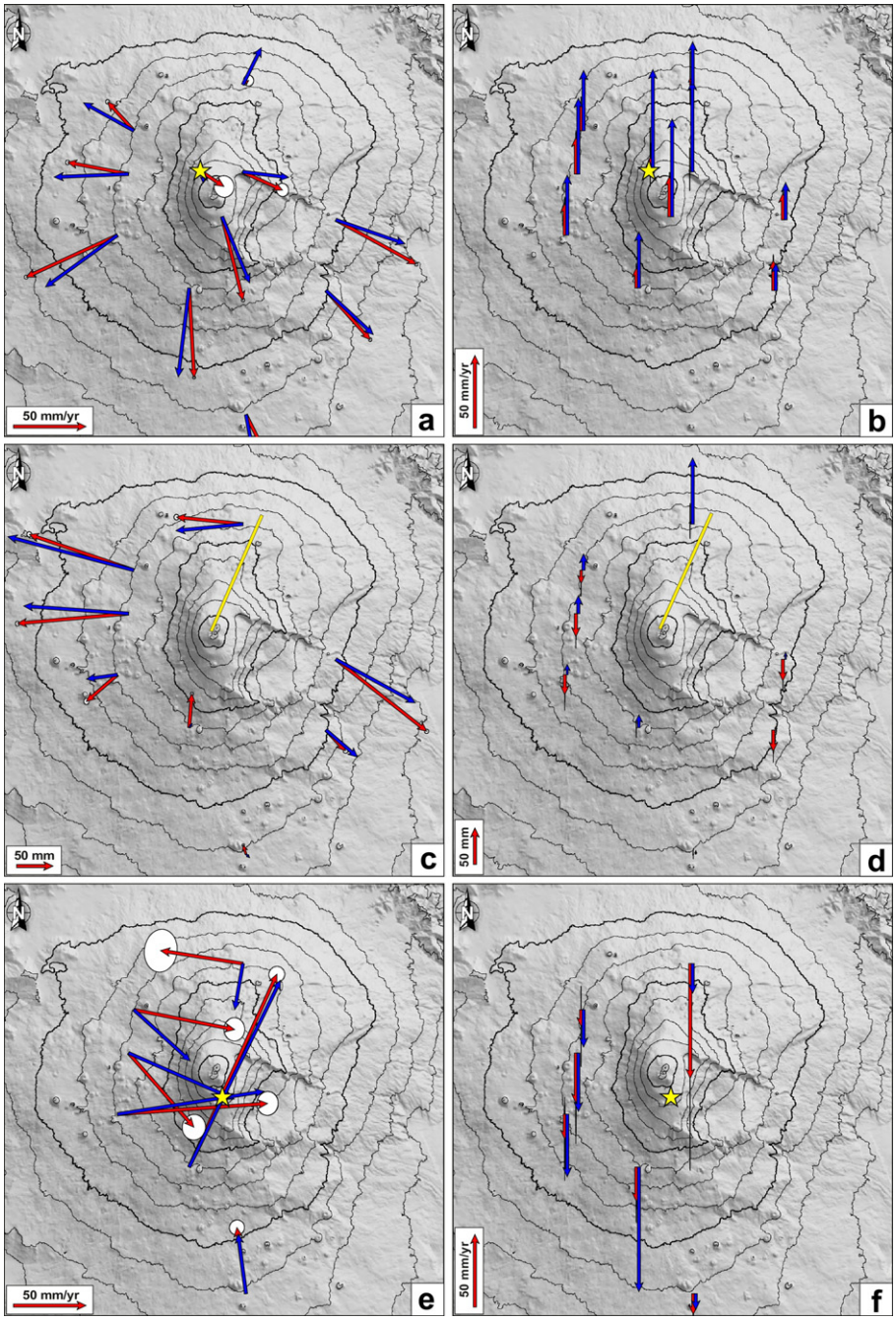

Fig. 3. Comparison between observed (red arrows) and modeled (blue arrows) horizontal (a, c and e) and vertical (b, d and f) deformation fields relevant to the considered time intervals:(a, b) for T1 (20 December 2001–26 October 2002), (c, d) for T2 (26–27 October 2002; to compute the amount of 3-D displacement during this interval, we estimated the average site position in the 2 days preceding the event and in the 2 days following by constraining translation, scale and rotation to 0.1 mm), (e, f) for T3 (27 October 2002–23 January 2003). The surface projections of modeled sources are reported as yellow stars/lines.

Variations during the whole 2002–2006 eruptive period have been evaluated in terms of some major (CaO/Al_2O_3 and Mg/FeO_{tot}) and trace (Th/La and Rb/Nb) element ratios, along with Sr-Nd-Pb isotope compositions (Figs. 6 and 7). Selection of these major element ratios gives a good indication on the degree of magma evolution, which is primarily influenced by fractional crystallization of olivine (silicate of Fe-Mg), clinopyroxene (silicate of Ca-Mg-Fe-Al) and plagioclase (silicate of Ca-Na-K-Al) in Etnean magmas. Ratios for trace elements have been selected considering elements with distinct geochemical behavior, i.e. Th markedly incompatible high field strength element (HFSE), Nb moderately incompatible high field strength element (HFSE), La incompatible element belonging to rare earth elements (REE), Rb incompatible element belonging to large ion lithophile elements (LILE). Among the isotope compositions, only Sr display a complete dataset that makes consistent the correlation for the whole 2002–06 period; Nd and Pb isotope compositions are fragmentary for the 2004–05 (Pb data are available only for a sample of the early activity) and the 2006 eruptions (Nd data are totally lacking).

Composition of the volcanic rocks erupted during the 2002–2006 period are classifiable as K-trachybasalts. They show generally similar petrographic characteristics to each other, except for products of the 2002–03 eruption. Volcanic rocks emitted during the 2002–03 eruption from the S-Rift are volatile-rich K-trachybasalts, peculiar for the rare occurrence (exclusively in the early erupted products) of destabilized

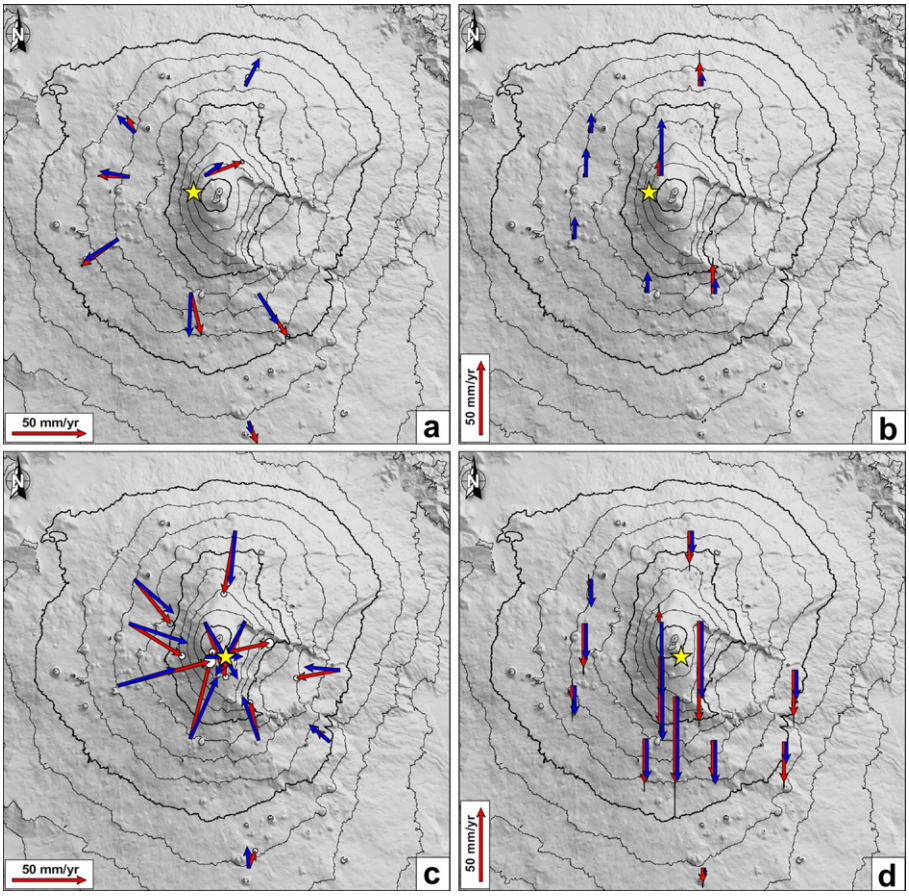

Fig. 4. Comparison between observed (red arrows) and modeled (blue arrows) horizontal (a and c) and vertical (b and d) deformation fields relevant to the considered time intervals: (a, b) for T4 (23 January 2003–7 September 2004), (c, d) for T4 (7 September 2004–10 March 2005). The surface projections of modeled sources are reported as yellow stars.

amphibole Mg-hastingsitic/pargasitic in composition (Clocchiatti et al., 2004; Ferlito et al., 2012), whereas those erupted along structures of the NE-Rift are amphibole-free. In recent periods, only the markedly volatile-rich products (H_2O = 3.4 wt%; cf. Métrich et al., 2004) erupted from the S-Rift during the July–August 2001 eruption displayed the uncommon presence of amphibole. Various authors interpreted this occurrence as due to peculiar crystallization conditions developed in cooler portions of a closed, overpressurized magma reservoir. Reaction corona of these Mg-hastingsitic/pargasitic amphiboles should have formed during pre-eruptive conditions as a response of fast decompression and/or increase of temperature due to mixing processes (Pompilio and Rutherford, 2002; Clocchiatti et al., 2004; Viccaro et al., 2007). K-trachybasalts erupted along structures of the S-Rift during the 2002–03 activity also show markedly different characteristics as concerns major-trace elements and isotope compositions if compared to those emitted throughout the 2002 eruptive activity at the NE-Rift (Figs. 6 and 7). CaO/Al_2O_3 and MgO/FeO_{tot} in all the considered datasets available for the 2002–03 activity give indications that products emitted from S-Rift structures are more basic than those from NE-Rift structures (Fig. 6). Ferlito et al. (2009), and later Giacomoni et al. (2014) on the same samples, highlighted that products feeding the eruptive activity along the NE-Rift were at least of three types on the basis of their petrographic vs. compositional characteristics (Fig. 6): 1) high potassium porphyritic lavas with phenocryst content of 20–32% and K_2O contents higher than 2 wt% (HKP in Ferlito et al., 2009); 2) lavas and tephra with low phenocryst volume < 20% and K_2O content higher than 2 wt% (HKO in Ferlito et al., 2009); 3) low potassium tephra with low modal phenocryst volume < 20% but K_2O content <2 wt% (LKO in Ferlito et al., 2009). The markedly different trace element and Sr-Nd-Pb isotope ratios of the 2002–03 S-Rift and 2002 NE-Rift products suggest that, in addition to the different degree of evolution, they also have distinct geochemical signatures (Figs. 6 and 7).

K-trachybasaltic products emitted during the early phases of the 2004–05 eruption in September show, on average, a slightly higher degree of evolution (lower MgO/FeO_{tot} and CaO/Al_2O_3; Fig. 6) than that of the last erupted products of the 2002–03 activity at the S-Rift [this characteristic is more emphasized considering the datasets of Clocchiatti et al., 2004 and Ferlito et al., 2012]. However, they are different with regard to either trace element or isotope ratios, being on average slightly enriched in Th/La, Rb/Nb, $^{87}Sr/^{86}Sr$ and depleted in $^{206}Pb/^{204}Pb$ (Figs. 6 and 7). Corsaro et al. (2009) presented a complete dataset for products of the 2004–05 activity, pertaining to various phases of the eruption. They highlighted that, throughout the eruption, the emitted magmas become more basic and have distinct trace elements and Sr-Nd isotope compositions (Pb cannot be evaluated through time; Figs. 6 and 7). This feature, although more discontinuously, is also observable from the

Fig. 5. Comparison between observed (red arrows) and modeled (blue arrows) horizontal (a, c, e and g) and vertical (b, d, f and h) deformation fields relevant to the considered time intervals: (a, b) for T6 (10 March 2005–12 November 2005), (c, d) for T7 (12 November 2005–6 March 2006), (e, f) for T9 (4 April 2006–13 October 2006), (g, h) for T10 (13 October 2006–16 December 2006). The surface projections of modeled sources are reported as yellow stars. The surface deformation observed during T8 (6 March 2006–4 April 2006) is reported in the supplementary material, as no consistent deformation pattern is discernible for it and no modeling was performed.

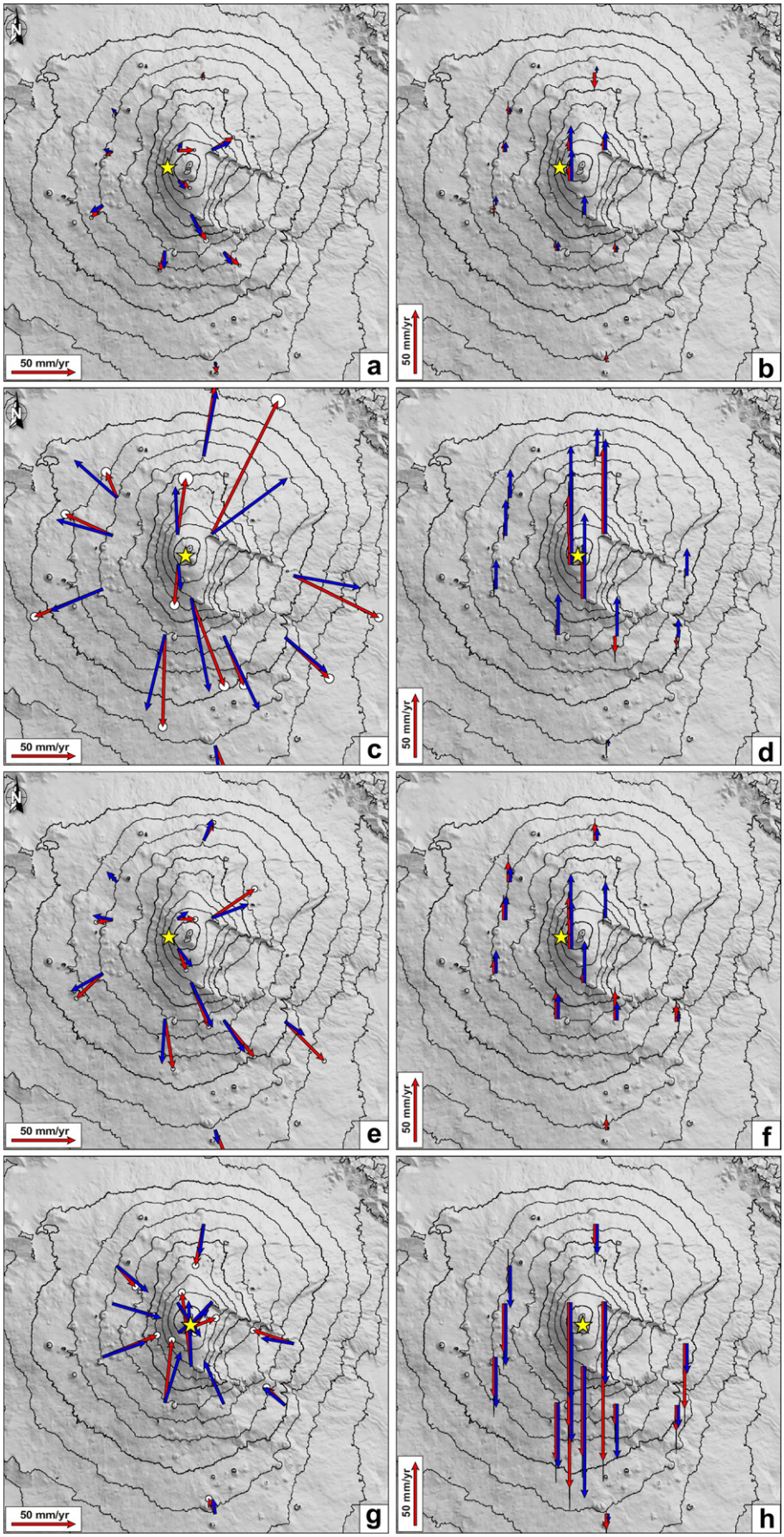
N
50 mm/yr
a
b
c
d
e
f
g
h

trace element dataset presented by Ferlito et al. (2012). In accordance with this evidence, Giacomoni et al. (2014) also observed a marked change in plagioclase textures found in products pertaining to various stages of the 2004–05 eruption, which suggest modification of the magma transfer dynamics at depth.

Compositional data for volcanic rocks of the 2006 eruptive period are only available from Nicotra and Viccaro (2012). The comparison of this dataset with those by Corsaro et al. (2009) and Ferlito et al. (2012) revealed that MgO/FeO_{tot} and CaO/Al_2O_3 of K-trachybasaltic magmas emitted in July 2006 (early phase of the eruption) are considerably lower with respect to those of the last erupted lavas of 2005 (Fig. 6). This suggests a general more evolved character of the 2006 magmas at the beginning of the activity. Geochemical differences are maintained also looking at trace element ratios [higher Rb/Nb and lower Th/La than Ferlito et al., 2012 and, to a less extent, than those by Corsaro et al., 2009; Fig. 6]. Values of the $^{87}Sr/^{86}Sr$ ratio at the end of 2005 and beginning of 2006 activities are mostly comparable (Fig. 7). These characteristics of trace elements and isotope ratios are kept rather constant throughout the 2006 eruption course (Figs. 6 and 7), although some subtle variations have led Nicotra and Viccaro (2012) to hypothesize that the eruptive picture changed from a petrological standpoint around the second half of October. Indeed, during this phase of the eruption, products record more scattered values for both trace element ratios and Sr-Pb isotope compositions (Figs. 6 and 7), suggesting the involvement of a geochemically-distinct magma than that erupted from July until the first half of October. Nicotra and Viccaro (2012), and Giacomoni et al. (2014) on a more limited sample dataset, observed changes in the frequency and types of equilibrium/disequilibrium textures in plagioclase crystals throughout the 2006 eruption course, which on the whole are in accordance with the geochemical modifications of the magma.

5. Discussion

In the following we discuss the results and compare the geodetic and petrological data for all the inflation/eruption/deflation cycles detected. It must be noted that, the volatile phases in the magmatic system should be considered as a possible source of deformation, especially during an inflation process. While the deflation of a volcano edifice is primary due to fluid/gas discharge, the inflation process can be explained either by input of new magma into the reservoir or by exsolution and boiling of volatile phases in the reservoir (e.g., Aloisi et al., 2011; Palano et al., 2012). In the former case, the inflation should be related to the drop in pressure in the magmatic reservoir which creates a pressure imbalance with a deeper magma source. This pressure imbalance motivates ascent of fresh magma from the deep source into the reservoir. In the latter case, decompression of the magmatic reservoir, due to magma discharge, can promote selective volatile exsolution and boiling, depending on their solubilities (e.g. Carroll and Holloway, 1994; Métrich and Mandeville, 2010). Moreover, volatile phases passing through magmas along the plumbing system can reach saturation and bring also about magma overpressure (Aloisi et al., 2011). In the following, we refer to the detected sources of inflation as due to magma overpressure in order to provide a simplified view on the magma transport and storage at Mt. Etna.

For what regards the petrological constraints, we have integrated various recent findings achieved for Etna magmas (Ferlito et al., 2012; Giacomoni et al., 2014; Kahl et al., 2015; Mollo et al., 2015). Giacomoni et al. (2014) provided thermobarometric determinations on plagioclase crystals to fix their chemical and physical conditions of crystallization in the period 2001–2006. Nevertheless, their constraints should be considered valid only for growth textures or for those developed under minor disequilibrium; conversely, thermodynamic constraints must be considered cautiously for textures formed under strong disequilibrium, as they have been assumed at equilibrium in the modeling. Other valuable efforts to fix the physical and chemical conditions of crystallization of Mt. Etna magmas have been recently proposed by Mollo et al. (2015), who provided a series of experimentally-determined P-T-H_2O-fO_2 conditions related to the crystallization path of mineral phases found in the 2001–2012 products. However, the range of parameters proposed by Mollo et al. (2015) is too much wide to resolve with a certain detail the physical and chemical crystallization conditions of the 2002–2006 lavas. Based on the olivine compositions, Kahl et al. (2015) provided rigorous constraints on the magmatic environments of crystallization for various Etnean magmas emitted in the period 1991–2008. Although their set of thermodynamic parameters is very accurate, we cannot entirely use them for the temporal reconstruction of the magmatic events in the 2002–2006 period, basically due to the lack of a dense sampling (the 2004–05 eruption was not considered in Kahl et al., 2015).

5.1. December 2001–January 2003 cycle

After the end of the July–August 2001 eruptive event, GPS measurements clearly showed that Mt. Etna started inflating (T1), leading to two shallow dyke intrusions on the evening of 26 October 2002 (T2) and, subsequently, to a volcano-wide deflation (T3).

More in detail, the ground deformation field observed during T1 is characterized by a radial pattern of surface displacement of the volcano with vertical variations (e.g. uplift) exceeding 65 mm/yr on the summit area (Fig. 3a,b). The best model for this stage is given by a source located at a depth of ~7 km bsl and centered a few kilometers NE-ward of the summit area (Fig. 3a,b). Such a source has a prolate spheroid shape, dipping ~60° S-ward and is characterized by a positive volume change of $\sim 26.8 \times 10^6$ m^3 (Table 1).

During T2, the ground deformation pattern indicates a clear response of the volcano edifice to the dyke intrusion occurring beneath the NE-Rift area (Fig. 3c,d). Highest deformations have been measured at ETDF (~0.65 m) and EPDN (~1.15 m) stations, located close to the surface fracture fields opened during the dyke intrusion. Deformations with horizontal displacements of ~160 mm and ~60 mm have been measured for the northern half and the southern half of the volcano, respectively (Fig. 3c,d). The vertical component showed very small positive changes, from a few mm up to 30 mm. The large displacements measured at ETDF and EPDN stations have been removed from the model computation since their motion cannot be considered purely elastic. The modeled source is given by a near vertical dyke striking about N20°E and characterized by a length of ~7.7 km and a width of ~1.4 km (Table 1), denoting well the onset of seismic events occurring during the intrusion (Barberi et al., 2004). Aloisi et al. (2003), in modeling the ground deformation pattern measured by GPS and tilt stations, inferred a composite intrusion consisting of a vertical ascending dyke in the upper S-Rift and a lateral intrusion propagating along the NE-Rift. Here, the inversion of the GPS data only allows inferring the dyke intrusion occurring along the NE-Rift, while the dyke intruding along the S-Rift is poorly constrained. On the other hand, our model is able to explain most of the observed ground deformation, suggesting that the amount of deformation related to the S-Rift intrusion is confined closely to the opened eruptive field and poorly detectable by the GPS network. This fact, coupled with the low level of co-intrusion seismicity beneath the upper southern flank, would support a dyke emplacement occurring along a weakness zone crossing the S-Rift area (Carbone et al., 2014) and already fractured during the July–August 2001 eruption (González and Palano, 2014).

The deflation of the volcano edifice (T3) began simultaneously with the lava emission. The associated deformation field reveals that the pattern of the deflation was not purely elastic, probably due to the seaward motion of the eastern flank of the volcano (Palano et al., 2009) and other local inelastic effects (e.g. dyke closure due to waning magma pressure, surface fractures). Keeping in mind these possible problems, we attempted to model the observed ground deformation field. The best model is given by an elongated spheroid, which is located beneath the

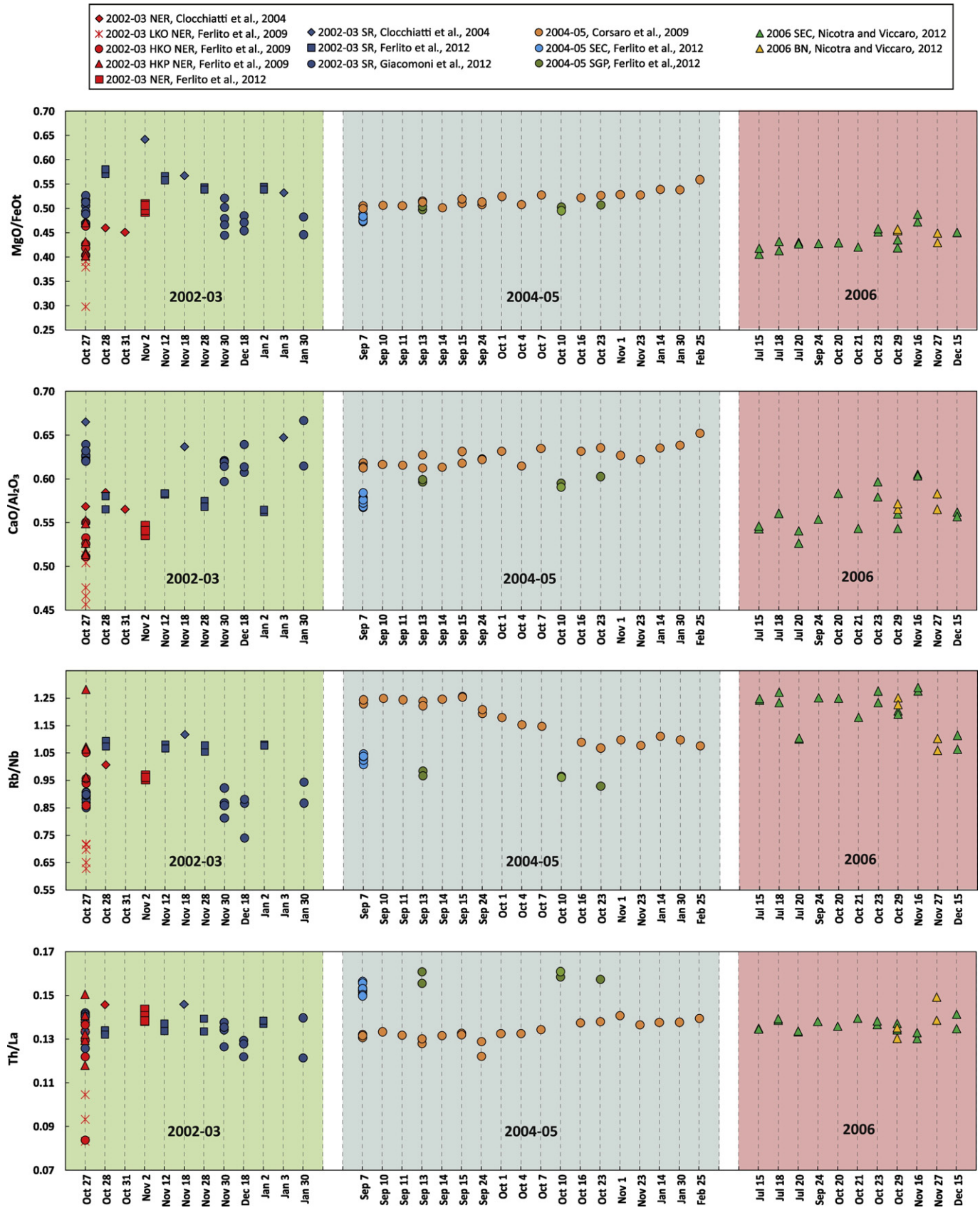

Fig. 6. Variations of selected major (Mg/FeO_{tot} and CaO/Al_2O_3) and trace (Rb/Nb and Th/La) element ratios during the 2002–2006 volcanic activity (time not in scale). Products of 2004–05 eruption from Ferlito et al. (2012) and Corsaro et al. (2009) show a similar trend, although the differences are due to different analytical laboratories. NER: North-East Rift; SR: South Rift; SEC: South-East Crater; BN: Bocca Nuova; SGP: Serra Giannicola Piccola; LKO: low potassium oligo-phyric volcanic products; HKO: high potassium oligo-phyric volcanic products; HKP: high potassium porphyritic volcanic products.

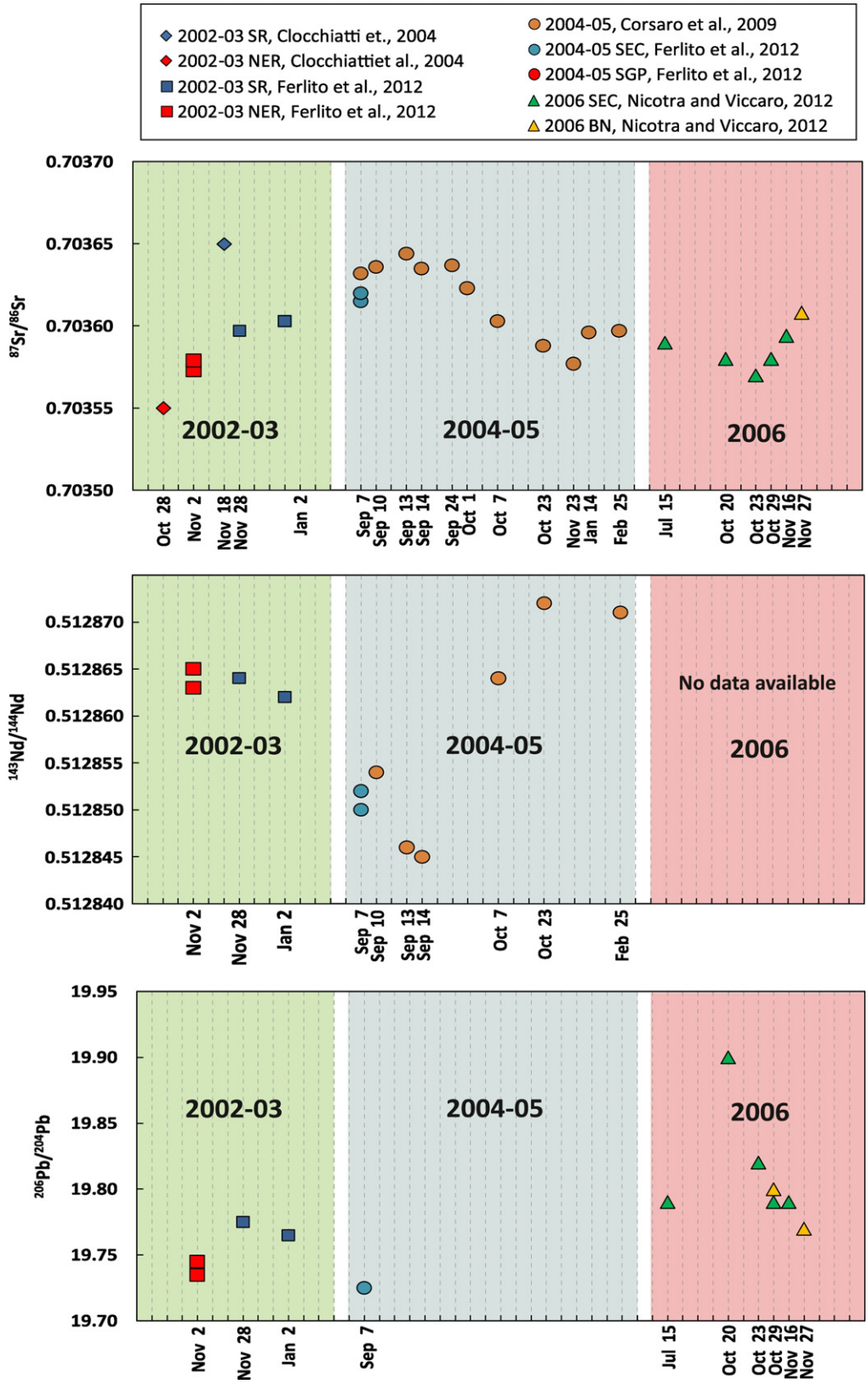

Fig. 7. Variations of Sr-Nd-Pb isotopic composition during the 2002–2006 volcanic activity (time not in scale). Sr shows a complete dataset for the time interval considered, while Nd—Pb data are fragmentary for 2004–05 and 2006 eruptions.

S-Rift area (Fig. 3e,f) at a depth of ~4.8 km bsl, dipping ~50° southward and is characterized by a negative volume change of ~7.3 × 10^6 m^3 (Table 1). Such a source may reasonably fit the ground deformation field measured at the GPS station located in the southern half of the volcano edifice, while the deformation at the remaining stations is poorly constrained. An additional source located beneath the NE-Rift might

improve the fit; however, the limited number of GPS stations on this side of the volcano does not enable adequately constraining the source parameters.

As previously mentioned, this eruptive event was characterized during (T2) by a contemporaneous intrusion in the upper S-Rift and along the NE-Rift. All the available petrological data indicated that the intrusion rising along the S-Rift was fed by volatile-rich (H_2O ~ 3.4 wt%; see Spilliaert et al., 2006 for details), fast-rising magma that drained a deep portion of the feeding system, which was in part residual and mixed with magma feeding the previous 2001 eruption (Clocchiatti et al., 2004; Ferlito et al., 2012). These features have been defined for the presence of destabilized Mg-hastingsitic/pargasitic amphibole in products of 2001 and in the early erupted lavas of 2002 from the S-Rift, together with mixed characteristics shown particularly by trace elements and Sr-Nd-Pb isotope ratios (Figs. 6 and 7). Therefore, this evidence supports the idea that volatile-rich products emitted during the 2001 and early 2002–03 eruptions from the S-Rift rose from a common deep magma reservoir. Indeed, the source inferred for T1, located beneath the upper western flank of Mt. Etna, at a depth of ~7 km bsl could be considered as the magmatic reservoir feeding the intrusion occurring along the S-Rift. In agreement with the geodetic observations, thermodynamic constraints provided by Ferlito et al. (2012) through MELTS simulations indicate crystallization conditions for this magma at temperature of 1100C°, pressure around 250–300 MPa, fO_2 at the QFM buffer and water of 3.4 wt%. Giacomoni et al. (2014) reported thermobarometric data obtained on plagioclases found in the S-Rift products, suggesting crystallization conditions as follows: temperature ~ 1130 °C, pressure 180–260 MPa, fO_2 at the QFM + 1 buffer and water of 1.7–2.3 wt%. Kahl et al. (2015) suggested that crystallization of olivines found in the 2002 products emitted at the S-Rift reflects crystallization in various magmatic environments (i.e., M0 for olivine $Fo_{79–83}$; M1 olivine $Fo_{75–78}$; M2 olivine $Fo_{70–72}$), whose chemical and physical parameters are the following: M0 = temperature > 1110 °C, pressure 300 MPa, fO_2 at the QFM–NNO buffers and water >3.5 wt%; M1 = temperature 1110–1080 °C, pressure 200–25 MPa, fO_2 at the QFM - NNO buffers and water <3.5 wt%; M2 = temperature 1080 °C, pressure 75–5 MPa, fO_2 at the QFM buffer and water 0.2–1.1 wt%. Despite the sometimes contrasting chemical and physical crystallization conditions provided by the previous authors, all of them make possible the crystallization of the magmas emitted at the S-Rift at pressure around 200–300 MPa, which are consistent with depths of ~6–7 km in accordance to what has been determined by geodetic data. Moreover, this source is closely located to the one detected before the onset of the July–August 2001 eruption (González and Palano, 2014); within the estimated uncertainties, both sources spatially overlap and, therefore, these sources can reasonably be considered the pressurizing of the same magmatic reservoir.

Interestingly, some textural and micro-analytical data on plagioclase crystals led Giacomoni et al. (2014) to fix at pressure of 70–150 MPa and water contents of 2.7–3.0 wt% the crystallization conditions of the early erupted products at the NE-Rift. In this regard, also Kahl et al. (2015) have found a rather shallow magmatic environment of crystallization for the early erupted lavas at the NE-Rift, although they emphasized a rather degassed nature of these products (water contents at 0.2–0.4 wt%). Conversely, lavas emitted at the end of the activity at the NE-Rift share a common history of crystallization with products emitted at the S-Rift, which was constrained by Giacomoni et al. (2014) in the pressure range of 180–260 MPa. This suggests that the intrusion along the NE-Rift during the early eruptive phases was fed by a magma stored at shallow levels (<3 km bsl) that evolved under different chemical-physical conditions, in order to justify its heterogeneous petrographic and chemical features (cf. Ferlito et al., 2009). Following Andronico et al. (2005), Ferlito et al. (2012) and Kahl et al. (2015), this magma was also partially degassed. Although the ground deformations measured during T3 do not allow constraining the reservoir feeding the eruptive fissures opened along the NE-Rift, the presence of a shallow reservoir cannot be excluded, since the evidence of shallow magmatic reservoirs (located beneath the summit area of the volcano) has been inferred by geodetic data before and during the July–August 2001 eruption (González and Palano, 2014).

5.2. January 2003–March 2005 cycle

A few weeks after the end of the 2002–03 eruption, a volcano-wide inflation (T4) began (Fig. 4a,b). The ground deformation field observed during this time interval is characterized by a weak pattern of surface deformation (values lower than 30 mm/yr) and culminated on 7 September 2004 with the resuming of volcanic activity at the base of the SE Crater (SEC) at ~3000 m asl. The modeling of this long lasting inflation (~590 days) infers a source located at a depth of ~4.3 km bsl centered a few kilometers west of the summit area and characterized by a positive volume change of ~13.4×10^6 m^3 (Table 1).

During T5, the volcano deflated due to magma drainage from the two vents opened on the upper western rim of the VdB (Fig. 4c,d). The modeling of the observed ground deformation pattern infers a source located at a depth of ~5.4 km bsl centered beneath the southeastern sector of the summit area and characterized by a negative volume change of ~8.2×10^6 m^3 (Fig. 4c,d and Table 1).

Sources inferred during T4 and T5 are similar to those reported in Bruno et al. (2012) in modeling the same time intervals. Some differences arise when parameters like “Pressure change”, “a/b ratio” and “Volume change” are compared (see Table 1 for explanation of parameters). These differences are related to the different upper limit of the ratio of pressure change to shear modulus and the value of the effective shear modulus adopted during the inversions and the volume change estimations, respectively. Considering the sources inferred in this study for this cycle of the volcano, some interesting considerations can be made. First of all, both sources do not spatially overlap and, therefore, could be considered two different magmatic reservoirs or two different portions of a large magmatic reservoir. Secondly, the deflation source (T5) is spatially overlapped with the source deflating during T3, but it is ~1.1 km deeper than the one inferred during the inflation stage T4.

The petrological observations made on products emitted during this T5 suggest a changed scenario with respect to the previous 2002–03 bilateral eruption (Figs. 6 and 7). Indeed, lavas of the 2004–05 eruption have a different geochemical signature if compared with lavas emitted either from the NE-Rift or from the S-Rift during the 2002–03 eruptive event (e.g. Corsaro et al., 2009; Ferlito et al., 2012). These authors explain this as due to progressive mixing between a residual magma with features like those of magmas feeding the 2003 activity from the S-Rift and a new, geochemically distinct magma intruding into the central conduits before the 2004–05 eruption onset. Occurrence of mixing is also supported by finding of dusty textures at rim of plagioclase crystals of the late volcanic activity (Giacomoni et al., 2014). On the basis of thermodynamic simulations through MELTS, Ferlito et al. (2012) reproduced the crystallization conditions of the 2004–05 lavas at temperature = 1100C°, pressure = 50 MPa, fO_2 at the QFM buffer and water no >2.5 wt%. Giacomoni et al. (2014) revised these constraints through thermobarometric determinations on plagioclase crystals, providing physical and chemical conditions that are in accordance with two crystallization scenarios belonging to different stages of the eruption. Plagioclases of the early erupted products would be crystallized at temperature 1080–1060 °C, pressure of 60–130 MPa, fO_2 at the QFM + 1 buffer and water 2.6–3.0 wt%, whereas those of the late activity at temperature 1110 °C, pressure of 150–200 MPa, fO_2 at the QFM + 1 buffer and water of 2.4–2.7 wt%.

All the available data match well with results inferred by the geodetic modeling, clearly highlighting that, during T4, a batch of fresh magma intruded into a magmatic reservoir located at a depth of ~4.3 km bsl and progressively mixed with the residual magma stored in the reservoir detected during T3. This gradual mixing favored a steady-state degassing and crystallization scenario. This produced a progressive

loss of volatiles, leading to a totally effusive eruption during T5, and consequently, to the depressurization of this magmatic reservoir.

5.3. March 2005–December 2006 cycle

After the end of the 2004–2005 eruption, a new inflation of the volcano edifice took place. As evidenced by the baseline time series reported in Fig. 2, the inflation was not constant over time, allowing the subdivision into different stages. Such a subdivision is different from the one reported in Bruno et al. (2012), where a unique long time interval has been considered. We observed a weak pattern of surface deformation during T6 (values of ~12.5 mm/yr on average for the horizontal components), changing to a marked one during T7 (values of ~54.8 mm/yr on average for the horizontal components). After a short period without a consistent deformation pattern (T8; the surface deformation observed during this period is reported in Fig. S2 of the supplementary material), a new moderate volcano-wide inflation took place until early October (T9), when a well-defined deflation of the volcano started (T10).

The best model inferred for T6 is given by an elongated spheroid which is located at a depth of ~4.5 km bsl and centered a few kilometers west of the summit area (Fig. 4a,b and Table 1). The sources inferred for intervals T7 (Fig. 4c,d) and T9 (Fig. 4e,f) have a similar shape and are located close to the one inferred for T6. As no consistent deformation pattern is discernible for interval T8, we chose not to perform any modeling. Taking these results into account, we suggest that these sources belong to the same magmatic reservoir; this reservoir, over the investigated interval was near-continuously recharged (with the exception of T8, where no clear information can be deduced), from depth at different rates. Moreover, the inflation observed during T9 was accompanied by some eruptive events at SEC (July–September 2006) that fed a number of lava flows (Fig. 2). This fact suggests that during T9, the reservoir was recharged from depth at a moderate but sustained rate. The source inferred for T10, spanning the 13 October - 16 December 2006, is located at a depth of ~3.7 km bsl beneath the SEC and was characterized by a negative volume change of ~4.6 $\times 10^6$ m^3 (Fig. 4g,h and Table 1).

From a petrological viewpoint, Nicotra and Viccaro (2012) evidenced that volcanic products emitted in July–December 2006 have some variations throughout the eruption (Figs. 6 and 7). On the basis of crystal fractionation simulations, they proposed that products erupted at the beginning of the 2006 eruption (14–24 July) have compositional affinities with products of the late 2005 eruption. Indeed, considering the products emitted after 25 February 2005 (Corsaro et al., 2009), the July 2006 products can be reproduced through subtraction of 10 vol% augitic clinopyroxene, 3 vol% plagioclase, 3 vol% olivine and 1 vol% Ti-magnetite from this composition (cf. Nicotra and Viccaro, 2012). Giacomoni et al. (2014) provided fragmentary thermobarometric data for plagioclase found in products of the 2006 eruptive episodes, which do not allow precise constraining of the physical and chemical conditions of crystallization throughout the complex course of events occurred between July and December. Kahl et al. (2015) indicate rather shallow crystallization conditions for the olivine core populations found in a sample emitted on July 2006 (magmatic environment M2 = temperature 1080 °C, pressure 75–5 MPa, fO_2 at the QFM buffer and water 0.2–1.1 wt%). In agreement with these constraints, Collins et al. (2009) also suggested that these features can only be achieved if the July 2006 magmas lost a considerable amount of their volatile load with respect to products of the previous eruptions (i.e. water concentrations <2 wt%). Thus, early-erupted lavas of July 2006 can be considered the residue from drainage of de-hydrated magma already occupying the open-conduit system since February–March 2005, whose eruption was triggered by new magma injections testified by the inflating periods T6, T7 and part of T9 (Fig. 4). The petrological scenario drastically changed in the second half of October 2006, when magma characterized by different Sr and Pb isotope signature with respect to the 2004–05 and the early-erupted lavas of 2006, began erupting from the active vents. In agreement with this observation, Kahl et al. (2015) provided evidence that the dominant olivine populations in these products (sample of October 28, 2006) are more forsteritic ($Fo_{79–83}$), which are representative of crystallization in a deeper magmatic environment (i.e., M0 = temperature > 1110 °C, pressure 300 MPa, fO_2 at the QFM–NNO buffers and water >3.5 wt%). This new, geochemically-distinct magma, which was emitted until the eruption end in December, could be correlated with the new moderate trend of inflation observed since the end of August (Fig. 2).

5.4. Constraints on the magma transport and storage at Mt. Etna

Inversion of surface deformation patterns allowed identification of the main pressurizing/depressurizing magmatic sources active during August 2001–December 2006. Also taking into account the sources inferred before and during the 2001 July–August eruption (see González and Palano, 2014 for details), we observed that all these sources are vertically distributed into two main groups (Fig. 8): one group is located close to a depth of ~7.2 km bsl, while the other one lies in the 3.5–5.5 km bsl depth interval. The former group is constituted by the two sources inferred for the 2001 eruption and by the source inferred for T1, while the latter group is defined by all the sources modeled since late October 2002. This fact suggests also a temporal subdivision between the two groups as discussed below. Moreover, an additional subdivision in the groups lying in the 3.5–5.5 km bsl depth interval can be observed: the pressurizing sources are located in the western side, while the depressurizing ones are located in the eastern side.

Modeled sources are located along the north-western border of a high seismic velocity zone (Fig. 8) supporting the hypothesis that

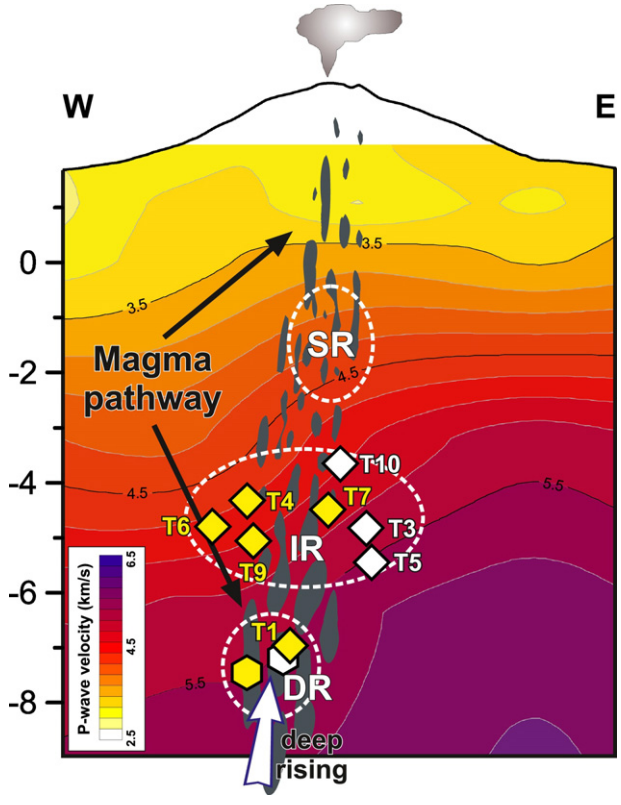

Fig. 8. Simplified sketch model of the Mt. Etna plumbing system. Sources modeled in this study (diamonds) as well as those inferred for the 2001 eruption (hexagons; González and Palano, 2014) are reported: inflating sources are colored in yellow while the deflating ones are in white. P-wave velocity tomography is reported as background (Chiarabba et al., 2000). SR: shallow reservoir; IR: intermediate reservoir, DR; deep reservoir (see the text for explanation).

magma preferentially rises along this pathway as already suggested by other investigators (e.g. Patanè et al., 2003; Bonforte et al., 2008; Palano et al., 2008 and references therein). We suggest that our source groups define two main reservoirs located at different depths along such a pathway. Based on their different depths along the magmatic pathway, in the following we refer to them using the terms "deep" and "intermediate". The deep reservoir, located at a depth of ~7 km bsl (according to our results) or slightly deeper (e.g. Puglisi and Bonforte, 2004), has occasionally been detected during the last two decades (e.g. Palano et al., 2008; Cannata et al., 2015). We suggest that such a deep reservoir can be considered as the crustal volume where basic magmas are accumulated. This reservoir appears connected with the intermediate reservoir located in the 3.5–5.5 km bsl depth interval as evidenced by the inflation/deflation patterns observed before and during the 2002–03 eruption. The intermediate reservoir would be considered as a permanent zone of magma storage, corresponding to a crustal level where the magma density equals that of the surrounding host rock. A small magmatic reservoir (SR in Fig. 8), located at shallower depth (<3 km bsl), inferred for the July–August 2001 eruption (by geodetic data; González and Palano, 2014) and believed to feed the 2002–03 eruption along the NE-Rift intrusion (by petrological observations; Ferlito et al., 2009; Giacomoni et al., 2014), completes the picture of the multi-level plumbing system of Mt. Etna volcano. Such a small reservoir, feeding also short-term volcanic activity (e.g. Strombolian and fountaining events), is considered a persistent feature of the shallow magmatic plumbing system of the volcano (Greco et al., 2016).

Geodetic and petrologic data analyzed in this study have enabled giving an improved picture about magma transport during the investigated time interval. After the end of the 2001 eruption, a fresh batch of magma entered into the feeding system leading to the pressurization of the deep reservoir and inflation of the volcano edifice (T1; Fig. 9a). This fresh magma mixed, in the deep reservoir, with the magma feeding the previous 2001 eruption. A batch of this magma ascended through the plumbing system into the shallower reservoir (<3 km bsl), where it evolved under different chemical-physical conditions (Fig. 9b). The sudden seaward motion (~3 cm) of the eastern flank of the volcano, observed a month before the eruption onset (e.g. Bonforte et al., 2007a), might have weakened the shallow crust beneath the summit area and along the NE-Rift, facilitating the magma ascent from the deep reservoir into the shallower one. In late October 2002, magma directly rose from the deep reservoir as well as from the shallow one toward the surface, leading to the eruptive activity along the S-Rift and the NE-Rift, respectively (T2; Fig. 9c). Gravity measurements, carried out along the NE-Rift, observed a 'pure' mass increase, i.e. a phenomenon likely due to filling of pre-existing voids (Bonforte et al., 2007b), therefore supporting our hypothesis of a weak shallow crust with enhanced porosity beneath the summit area and along the NE-Rift. During the course of the eruption, the drainage of magma from both the deep and the shallow reservoirs led to a pressure decrease and deflation of the volcano (T3; Fig. 9d).

A few weeks after the end of the 2002–03 eruption, fresh magma was supplied into the intermediate reservoir, leading to a slight inflation of the volcano (T4; Fig. 9e). We suggest that this new magma ascended from the deep reservoir into the intermediate reservoir. This hypothesis is supported by the lack of significant anomalies in the flux or composition of gas emitted from Etna in the year following the end of the 2002–03 eruption (Aiuppa et al., 2007). This magma progressively mixed with the residual one (T3) favoring a steady-state degassing and crystallization (Fig. 9f) and leading to an entirely effusive eruption during T5 (Fig. 9g). As highlighted by the baseline time series reported in Fig. 2, the inflation-rate slightly increased from early 2004, suggesting an increase in the influx of magma from depth. This magma, while still progressively mixing with the residual one, had passively pushed upward and gradually replaced the magma from the apical region of the reservoir toward the surface. Such a mechanism well explains the evidence that, throughout the eruption course, the emitted magmas gradually become more basic (e.g. Corsaro et al., 2009). The deflation of the volcano started contemporaneously with the effusion activity, in response of magma drainage from the intermediate reservoir (Fig. 9g).

After the end of the 2004–2005 eruption, a slight inflation of the volcano edifice took place (T6; Fig. 9h), highlighting that the magma reservoir was slightly pressurized. After mid-November 2005, the rate of the inflation increased, evidencing the arrival of a new batch of magma from depth. However, both T6 and T7 where characterized by a low value of the CO_2/SO_2 suggesting a partial closure of the pathway toward the surface (Aiuppa et al., 2007). The period between early March and early April 2006 (T8) was characterized by an inconsistent deformation pattern, although the selected baseline (Fig. 2) showed a slight shortening. However, from mid-April 2006, the inflation of the volcano resumed albeit occurring at a lower rate than the one observed during T7 (Fig. 9i). This new inflation is identified as the beginning of a new magma influx from depth as suggested from a sharp increase in CO_2/SO_2 data (Aiuppa et al., 2007). This period coincides with the observation of seismicity at 6–7 km depth (Alparone, 2006), which may have reactivated pathways that enabled magma and CO_2-rich gas to ascend to the surface. Moreover, this new magma pushed toward the surface and replaced the residual magma from the apical region of the reservoir, triggering the eruptive event occurring during 14–24 July (Fig. 9i). The volcanic activity restarted again at the end of August 2006. Since no change in the inflation rate was observed during these eruptive events, we suggest that the reservoir continued to be recharged from depth at least at the same rate (Fig. 9j). The deflation of the volcano started contemporaneously with the effusive activity of lava flows characterized by distinct geochemical signature, which were sometimes emitted with violent eruptive behavior (e.g. 16 November 16, 2006; see Ferlito et al., 2010 for details) from different fissure fields since mid-October 2006 (T10; Fig. 9k).

6. Concluding remarks

Continuous GPS measurements and petrological data collected at Mt. Etna during the mid-August 2001–December 2006 time interval have allowed providing new constraints on the spatial and temporal history of magma transfer and recharge within the plumbing system of the volcano. The inversion of geodetic data enabled identifying the magmatic reservoirs acting during the investigated interval. Although all the petrological constraints based on thermobarometric determinations and/or thermodynamic simulations suggest continuous crystallization of various mineral phases throughout the whole Etnean plumbing system (e.g. Kahl et al., 2011, 2013, 2015; Giacomoni et al., 2014; Mollo et al., 2015; Giuffrida and Viccaro, 2017), we have identified a source of deformation at a depth of ~7 km bsl, which can correspond to a preferential deep ponding level hosting poorly differentiated magmas. We also identified a shallower source of deformation located in the depth range of 3.5–5.5 km bsl, where preferential magma storage is probably favored due to neutral buoyancy between densities of the magma and the surrounding host rocks. This type of density balance promotes long-to-medium term magma residence (Viccaro et al., 2016a) and comprises an ideal depth interval for magma reservoir development. Through geodetic and petrological data we also fix the presence of a small magmatic reservoir located at a shallow depth (<3 km bsl), which usually fed short-term volcanic activity. The 2001 and 2002–03 eruptions along the S-Rift were fed by magma directly rising from the deep levels of the plumbing system, while the 2004–05 and 2006 eruptions were fed by magma rising from intermediate-shallower storage zones. This suggests that changes to the volcano's deep plumbing system might have occurred during the 2002–03 eruption and not after the 2004–05 eruption, as suggested by other authors (e.g. Bonforte et al., 2008). Indeed, the significant seaward motion of the eastern flank of the volcano occurring before and during the 2002–03 eruption onset (see Acocella et al., 2003; Palano et al.,

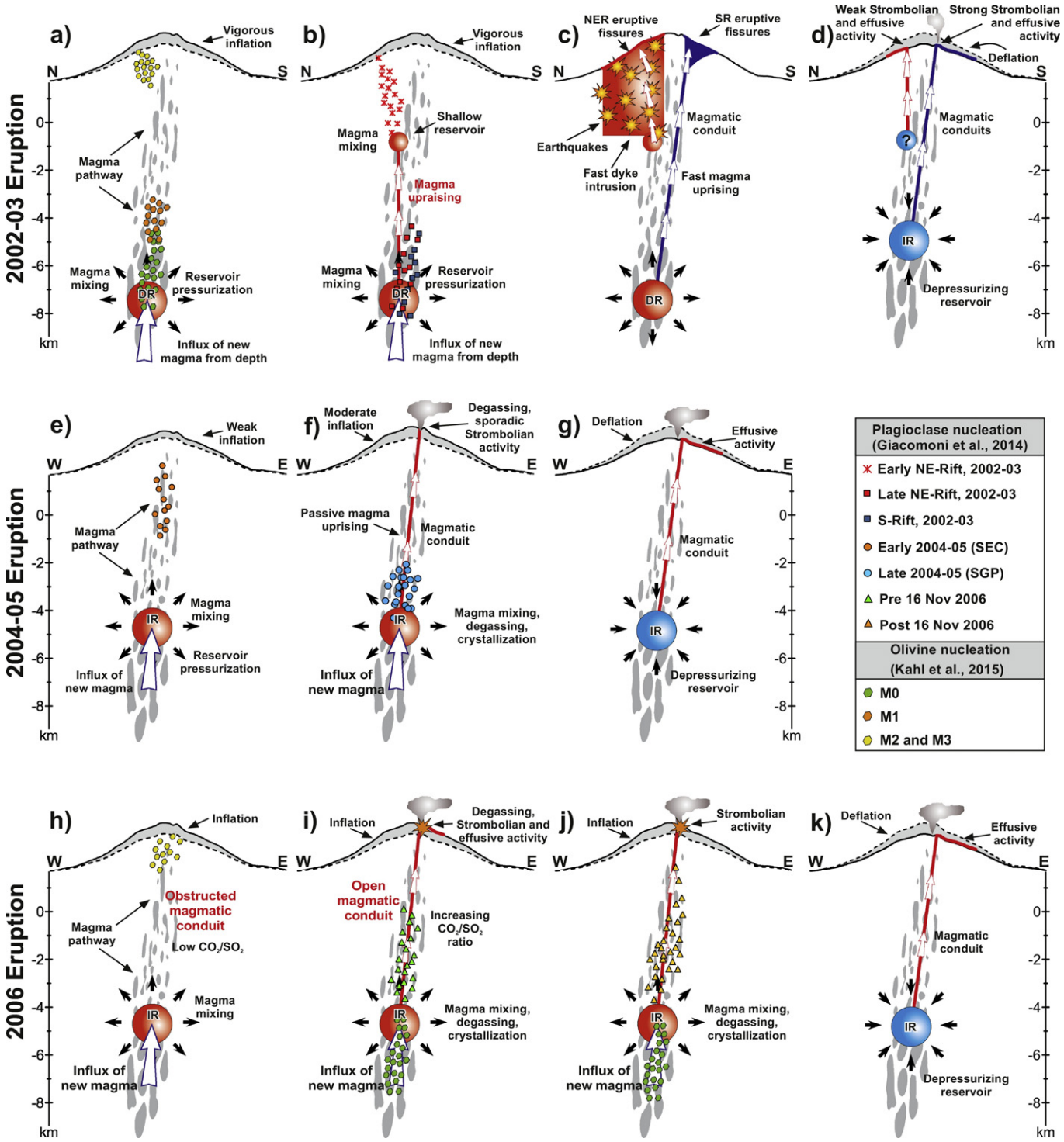

Fig. 9. Cartoons for the 2002–03 (panels a, b, c and d), 2004 (panels e, f and g) and 2006 (panels h, i, j and k) eruptive events. Inflating and deflating sources are reported in red and blue, respectively (IR, intermediate reservoir; DR, deep reservoir; see the text for explanation). Magma storages estimated from petrological data have been also added (see legend of figure for details; see also Fig. S3 in the supplementary material section for additional details). In panel c, the shallow magmatic source, highlighted with a question mark (the ground deformations do not allow constraining this reservoir), is believed to feed the 2002–03 eruption along the NE-Rift intrusion as suggested by petrological observations (Ferlito et al., 2009).

2009; for details) generated a W-E directed extension at the head of the sliding flank that presumably led to a decrease in the confining pressure and an increase in host-rock porosity. Such a mechanism enabled the formation of new pathways and may also provide a plausible explanation for eastward migration of these pathways (as suggested by the presence of deflating sources on the eastern side of the intermediate magmatic reservoir).

Acknowledgements

We are indebted to Daniele Pellegrino, Mario Pulvirenti and Massimo Rossi, technicians of the INGV - Osservatorio Etneo, who ensured the regular working of the continuous GPS stations. We thank the Editor in chief Alessandro Aiuppa and three anonymous referees for their useful comments and suggestions,

which helped us to significantly improve the early version of paper.

Appendix A. Supplementary data

Supplementary data to this article can be found online at https://doi.org/10.1016/j.jvolgeores.2017.09.009.

References

Acocella, V., Behncke, B., Neri, M., D'Amico, S., 2003. Link between major flank slip and 2002–2003 eruption at Mt. Etna (Italy). Geophys. Res. Lett. 30 (24):2286. https://doi.org/10.1029/2003GL018642.

Aiuppa, A., Moretti, R., Federico, C., Giudice, G., Gurrieri, S., Liuzzo, M., Papale, P., Shinohara, H., Valenza, M., 2007. Forecasting Etna eruptions by real-time observations of volcanic gas composition. Geology 35, 1115–1118.

Aloisi, M., Bonaccorso, A., Gambino, S., Mattia, M., Puglisi, G., 2003. Etna 2002 eruption imaged from continuous tilt and GPS data. Geophys. Res. Lett. 30 (23):2214. https://doi.org/10.1029/2003GL018896.

Aloisi, M., Mattia, M., Ferlito, C., Palano, M., Bruno, V., Cannavò, F., 2011. Imaging the multi-level magma reservoir at Mt. Etna volcano (Italy). Geophys. Res. Lett. 38: L16306. https://doi.org/10.1029/2011GL048488.

Alparone, S., 2006. Rapporto sull' attività sismica in Sicilia orientale: Settimana 24–30 Aprile 2006, INGV internal reportWKRSMREP20060512. Available at. http://www.ct.ingv.it/index.php?option=com_docman&Itemid=331&lang=it&limitstart=180, Accessed date: 5 September 2017.

Andronico, D., Branca, S., Calvari, S., Burton, M., Caltabiano, T., Corsaro, R.A., Del Carlo, P., Garfì, G., Lodato, L., Miraglia, L., Murè, F., Neri, M., Pecora, E., Pompilio, M., Salerno, G., Spampinato, L., 2005. A multi-disciplinary study of the 2002–03 Etna eruption: Insights into a complex plumbing system. Bull. Volcanol. 67:314–330. https://doi.org/10.1007/s00445-004-0372-8.

Barberi, G., Cocina, O., Maiolino, V., Musumeci, C., Privitera, E., 2004. Insight into Mt. Etna (Italy) kinematics during 2002–2003 eruption as inferred by seismic stress and strain tensors inversion. Geophys. Res. Lett. 31:L21614. https://doi.org/10.1029/2004GL020918.

Barnie, T.D., Keir, D., Hamling, I., Hofmann, B., Belachew, M., Carn, S., Eastwell, D., Hammond, J.O.S., Ayele, A., Oppenheimer, C., Wright, T., 2015. A multidisciplinary study of the final episode of the Manda Hararo dyke sequence, Ethiopia, and implications for trends in volcanism during the rifting cycle. Geol. Soc. Lond. Spec. Publ. https://doi.org/10.1144/SP420.6.

Bonforte, A., Gambino, S., Guglielmino, F., Obrizzo, F., Palano, M., Puglisi, G., 2007a. Ground deformation modeling of flank dynamics prior to the 2002 eruption of Mt. Etna. Bull. Volcanol. 69:757–768. https://doi.org/10.1007/s00445-006-0106-1.

Bonforte, A., Carbone, D., Greco, F., Palano, M., 2007b. Intrusive mechanism of the 2002 NE-Rift eruption at Mt. Etna (Italy) modelled using GPS and gravity data. Geophys. J. Int. 169:339–347. https://doi.org/10.1111/j.1365-246X.2006.03249.x.

Bonforte, A., Bonaccorso, A., Guglielmino, F., Palano, M., Puglisi, G., 2008. Feeding system and magma storage beneath Mt. Etna as revealed by recent inflation/deflation cycles. J. Geophys. Res. 113, B05406. https://doi.org/10.1029/2007jb005334.

Bruno, V., Mattia, M., Aloisi, M., Palano, M., Cannavò, F., Holt, W.E., 2012. Ground deformations and volcanic processes as imaged by CGPS data at Mt. Etna (Italy) between 2003 and 2008. J. Geophys. Res. 117, B07208. https://doi.org/10.1029/2011JB009114.

Cannata, A., Spedalieri, G., Behncke, B., Cannavò, F., Di Grazia, G., Gambino, S., Gresta, S., Gurrieri, S., Liuzzo, M., Palano, M., 2015. Pressurization and depressurization phases inside the plumbing system of Mount Etna volcano: evidence from a multiparametric approach. J. Geophys. Res. 120:5965–5982. https://doi.org/10.1002/2015JB012227.

Carbone, D., Aloisi, M., Vinciguerra, S., Puglisi, G., 2014. Stress, strain and mass changes at Mt. Etna during the period between the 1991–93 and 2001 flank eruptions. Stress, strain and mass changes at Mt. Etna during the period between the 1991–93 and 2001 flank eruptions. Earth Sci. Rev. 138:454–468 https://doi.org/10.1016/j.earscirev.2014.07.004.

Carroll, M.R., Holloway, J.R., 1994. Volatiles in magmas. Mineral. Soc. Am. Rev. Mineral. 30, 1–517.

Chiarabba, C., Amato, A., Boschi, E., Barberi, F., 2000. Recent seismicity and tomographic modeling of the Mount Etna plumbing system. J. Geophys. Res. 105 (B5): 10923–10938. https://doi.org/10.1029/1999JB900427.

Clocchiatti, R., Condomines, M., Guènot, N., Tanguy, J.C., 2004. Magma changes at Mount Etna: the 2001 and 2002–2003 eruptions. Earth Planet. Sci. Lett. 226, 397–414.

Collins, S.J., Pyle, D.M., Maclennan, J., 2009. Melt inclusions track pre-eruption storage and dehydration of magmas at Etna. Geology 37, 571–574.

Corsaro, R.A., Miraglia, L., 2005. Dynamics of 2004–2005 Mt. Etna effusive eruption as inferred from petrologic monitoring. Geophys. Res. Lett. 32, L13302. https://doi.org/10.1029/2005GL022347.

Corsaro, R.A., Civetta, L., Di Renzo, V., Miraglia, L., 2009. Petrology of lavas from the2004–05 flank eruption of Mt. Etna, Italy: inferences on the dynamics of magma in the shallow plumbing system. Bull. Volcanol. 71, 781–793.

Efron, B., 1982. The Jackknife, Bootstrap and Other Resampling Plans. Society for Industrial and Applied Mathematics, Philadelphia, PA.

Ferlito, C., Coltorti, M., Cristofolini, R., Giacomoni, P.P., 2009. The contemporaneous emission of low-K and high-K trachybasalts and the role of the NE Rift during the 2002 eruptive event, Mt. Etna, Italy. Bull. Volcanol. 67, 314–330.

Ferlito, C., Viccaro, M., Nicotra, E., Cristofolini, R., 2010. Relationship between the flank sliding of the South East Crater (Mt. Etna, Italy) and the paroxysmal event of November 16, 2006. Bull. Volcanol. 72, 1179–1190.

Ferlito, C., Viccaro, M., Nicotra, E., Cristofolini, R., 2012. Regimes of magma recharge and their control on the eruptive behaviour during the 2001–2005 period at Mt. Etna (Italy). Bull. Volcanol. 74, 533–543.

Gambino, S., Cannata, A., Cannavò, F., La Spina, A., Palano, M., Sciotto, M., Spampinato, L., Barberi, G., 2016. The unusual 28 December 2014 dike-fed paroxysm at Mount Etna: Timing and mechanism from a multidisciplinary perspective. J. Geophys. Res. Solid Earth 121:2037–2053. https://doi.org/10.1002/2015JB012379.

Giacomoni, P.P., Ferlito, C., Alesci, G., Coltorti, M., Monaco, C., Viccaro, M., Cristofolini, R., 2012. A common feeding system of the NE and S rifts as revealed by the bilateral 2002/2003 eruptive event at Mt. Etna (Sicily, Italy). Bull. Volcanol. 74, 2415–2433.

Giacomoni, P.P., Ferlito, C., Coltorti, M., Bonadiman, C., Lanzafame, G., 2014. Plagioclase as archive of magma ascent dynamics on "open conduit" volcanoes: The 2001–2006 eruptive period at Mt. Etna. Earth-Sci. Rev. 138, 371–393.

Giuffrida, M., Viccaro, M., 2017. Three years (2011 — 2013) of eruptive activity at Mt. Etna: working modes and timescales of the modern volcano plumbing system from micro-analytical studies of crystals. Earth-Sci. Rev. 171, 289–322.

González, P.J., Palano, M., 2014. Mt. Etna 2001 eruption: New insights into the magmatic feeding system and the mechanical response of the western flank from a detailed geodetic dataset. J. Volcanol. Geotherm. Res. 274:108–121. https://doi.org/10.1016/j.jvolgeores.2014.02.001.

Greco, F., Currenti, G., Palano, M., Pepe, A., Pepe, S., 2016. Evidence of a shallow persistent magmatic reservoir from joint inversion of gravity and ground deformation data: The 25–26 October 2013 Etna lava fountaining event. Geophys. Res. Lett. 3246–3253. https://doi.org/10.1002/2016GL068426.

Herring, T.A., King, R.W., McClusky, S.C., 2010. Introduction to GAMIT/GLOBK, Release10.4. Massachusetts Institute of Technology, Cambridge (MA 1–48).

Kahl, M., Chakraborty, S., Costa, F., Pompilio, M., 2011. Dynamic plumbing system beneath volcanoes by kinetic modeling, and the connection to monitoring data: an example from Mt. Etna. Earth Planet. Sci. Lett. 308, 11–22.

Kahl, M., Chakraborty, S., Costa, F., Pompilio, M., Liuzzo, M., Viccaro, M., 2013. Compositionally zoned crystals and real-time degassing data reveal changes in magma transfer dynamics during the 2006 summit eruptions of Mt. Etna. Bull. Volcanol. 75:692. https://doi.org/10.1007/s00445-013-0692-7.

Kahl, M., Chakraborty, S., Pompilio, M., Costa, F., 2015. Constraints on the nature and evolution of the magma plumbing system of Mt. Etna volcano (1991–2008) from a combined thermodynamic and kinetic modelling of the compositional record of minerals. J. Petrol. 56, 2025–2068.

Lisowski, M., Dzurisin, D., Denlinger, R.P., Iwatsubo, E.Y., 2008. Analysis of GPS-measured deformation associated with the 2004–2006 dome-building eruption of Mount St. Helens, Washington. In: Sherrod, R.D., Scott, W.E., Stauffer, P.H. (Eds.), A Volcano Rekindled: the Renewed Eruption of Mount St. Helens, 2004–2006. 1750. USGS, pp. 301–333 Prof. Pap.

Martí, J., Castro, A., Rodríguez, C., Costa, F., Carrasquilla, S., Pedreira, R., Bolos, X., 2013. Correlation of magma evolution and geophysical monitoring during the 2011–2012 El Hierro (Canary Islands) submarine eruption. J. Petrol. 54, 1349–1373.

Martini, F., Tassi, F., Vaselli, O., Del Potro, R., Martinez, M., Van del Laat, R., Fernandez, E., 2010. Geophysical, geochemical and geodetical signals of reawakening at Turrialba volcano (Costa Rica) after almost 150 years of quiescence. J. Volcanol. Geotherm. Res. 198, 416–432.

Métrich, N., Mandeville, C.W., 2010. Sulfur in magmas. Elements 6, 81–86.

Métrich, N., Allard, P., Spilliaert, N., Andronico, D., Burton, M.R., 2004. 2001 flank eruption of the alkali- and volatile-rich primitive basalt responsible for Mount Etna's evolution in the last three decades. Earth Planet. Sci. Lett. 228, 1–17.

Mollo, S., Giacomoni, P.P., Coltorti, M., Ferlito, C., Iezzi, G., Scarlato, P., 2015. Reconstruction of magmatic variables governing recent Etnean eruptions: constraints from mineral chemistry and P–T–fO_2–H2O modelling. Lithos 212–215, 311–320.

Nicotra, E., Viccaro, M., 2012. Transient uprise of gas and gas-rich magma batches fed the pulsating behavior of the 2006 eruptive episodes at Mt. Etna volcano. J. Volcanol. Geotherm. Res. 227–228, 102–118.

Okada, Y., 1985. Surface deformation due to shear and tensile fault in half-space. Bull. Seismol. Soc. Am. 75, 1135–1154.

Palano, M., Puglisi, G., Gresta, S., 2008. Ground deformation patterns at Mt. Etna from 1993 to 2000 from joint use of InSAR and GPS techniques. J. Volcanol. Geotherm. Res. 169 (3–4):99–120. https://doi.org/10.1016/j.jvolgeores.2007.08.014.

Palano, M., Gresta, S., Puglisi, G., 2009. Time-dependent deformation of the eastern flank of Mt. Etna: after-slip or viscoelastic relaxation? Tectonophysics 473:300–311. https://doi.org/10.1016/j.tecto.2009.02.047.

Palano, M., Rossi, M., Cannavò, C., Bruno, V., Aloisi, M., Pellegrino, D., Pulvirenti, M., Siligato, G., Mattia, M., 2010. Etn@ref, a geodetic reference frame for Mt. Etna GPS networks. Ann. Geophys. 53 (4):48–79. https://doi.org/10.4401/af-4879.

Palano, M., Guarrera, E., Mattia, M., 2012. GPS ground deformation patterns at Mount St. Helens (Washington, USA) from 2004 to 2010. Terra Nova 24:148–155. https://doi.org/10.1111/j.1365-3121.2011.01049.x.

Patanè, D., De Gori, P., Chiarabba, C., Bonaccorso, C., 2003. Magma Ascent and the pressurization of Mount Etna's Volcanic System. Science 299, 2061–2063.

Pompilio, M., Rutherford, M.J., 2002. Pre-eruption conditions and magma dynamics of recent amphibole-bearing Etna basalt. AGU, Fall Meeting Abstracts. 83, pp. 47–F1419.

Puglisi, G., Bonforte, A., 2004. Ground deformation studies on Mt. Etna from 1995 to 1998 using static and kinematic GPS measurements. J. Geophys. Res. 109:B11040 (doi: 10.1029.2003JB002878).

Saunders, K., Blundy, J., Dohmen, R., Cashman, K., 2012. Linking Petrology and Seismology at an Active Volcano. Science 336, 1023–1027.

Spampinato, L., Sciotto, M., Cannata, A., Cannavò, F., La Spina, A., Palano, M., Salerno, G.G., Privitera, E., Caltabiano, T., 2015. Multiparametric study of the February–April 2013 paroxysmal phase of Mt. Etna New South-East crater. Geochem. Geophys. Geosyst. 16:1932–1949. https://doi.org/10.1002/2015GC005795.

Spilliaert, N., Allard, P., Métrich, N., Sobolev, A.V., 2006. Melt inclusion record of the conditions of ascent, degassing, and extrusion of volatile-rich alkali basalt during the powerful 2002 flank eruption of Mount Etna (Italy). J. Geophys. Res. Solid Earth 111, B04203.

Tiampo, K.F., Rundle, J.B., Fernandez, J., Langbein, J.O., 2000. Spherical and ellipsoidal volcanic sources at Long Valley caldera, California, using a genetic algorithm inversion technique. J. Volcanol. Res. 102:189–206. https://doi.org/10.1016/S0377-0273(00)00185-2.

Viccaro, M., Ferlito, C., Cristofolini, R., 2007. Amphibole crystallization in the Etnean feeding system: mineral chemistry and trace element partitioning between Mg-hastingsite and alkali basaltic melt. Eur. J. Mineral. 19, 499–511.

Viccaro, M., Garozzo, I., Cannata, A., Di Grazia, G., Gresta, S., 2014. Gas burst vs. gas-rich magma recharge: A multidisciplinary study to reveal factors controlling duration of the recent paroxysmal eruptions at Mt. Etna. J. Volcanol. Geotherm. Res. 278–279, 1–13.

Viccaro, M., Barca, D., Bohrson, W.A., D'Oriano, C., Giuffrida, M., Nicotra, E., Pitcher, B.W., 2016a. Crystal residence times from trace element zoning in plagioclase reveal changes in magma transfer dynamics at Mt. Etna during the last 400 years. Lithos 248–251, 309–323.

Viccaro, M., Zuccarello, F., Cannata, A., Palano, M., Gresta, S., 2016b. How a complex basaltic volcanic system works: constraints from integrating seismic, geodetic, and petrological data at Mount Etna volcano during the July–August 2014 eruption. J. Geophys. Res. Solid Earth 121:5659–5678. https://doi.org/10.1002/2016JB013164.

Williams, C.A., Wadge, G., 2000. An accurate and efficient method for including the effects of topography in three-dimensional elastic models of ground deformation with applications to radar interferometry. J. Geophys. Res. 105 (B4):8103–8120. https://doi.org/10.1029/1999JB900307.

Yang, X.-M., Davis, P.M., Dieterich, J.H., 1988. Deformation from inflation of a dipping finite prolate spheroid in an elastic half-space as a model for volcanic stressing. J. Geophys. Res. 93, 4249–4257.